ACS OMEGA

Article

http://pubs.acs.org/journal/acsodf

In Situ Mg/MgO-Embedded Mesoporous Carbon Derived from Magnesium 1,4-Benzenedicarboxylate Metal Organic Framework as Sustainable Li−S Battery Cathode Support

Tanumoy Dhawa, Shreyasi Chattopadhyay, Goutam De,* and Sourindra Mahanty*

CSIR-Central Glass & Ceramic Research Institute, 196 Raja S.C. Mullick Road, Kolkata 700032, India

Supporting Information

ABSTRACT: Development of advanced carbon cathode support with the ability to accommodate high sulfur (S) content as well as effective confinement of the sulfur species during charge−discharge is of great importance for sustenance of Li−S battery. A facile poly(vinylpyrrolidone)-assisted solvothermal method is reported here to prepare Mg−1,4-benzenedicarboxylate metal organic framework (MOF) from which mesoporous carbon is derived by thermal treatment, where the hexagonal sheetlike morphology of the parent MOF is retained. Existence of abundant pores of size 4 and 9 nm extended in three dimensions with zigzag mazelike channels helps trapping of S in the carbon matrix through capillary effect, resulting in high S loading. When tested as a cathode for lithium−sulfur battery, a reversible specific capacity of 1184 mAh g^{-1} could be achieved at 0.02 C. As evidenced by X-ray photoelectron spectroscopy, in situ generated Mg in the carbon structure enhances the conductivity, whereas MgO provides support to S immobilization through chemical interactions between Mg and sulfur species for surface polarity compensation, restricting the dissolution of polysulfide into the electrolyte, the main cause for the "shuttle phenomenon" and consequent capacity fading. The developed cathode shows good electrochemical stability with reversible capacities of 602 and 328 mAh g^{-1} at 0.5 and 1.0 C, respectively, with retentions of 64 and 67% after 200 cycles. The simple MOF-derived strategy adopted here would help design new carbon materials for Li−S cathode support.

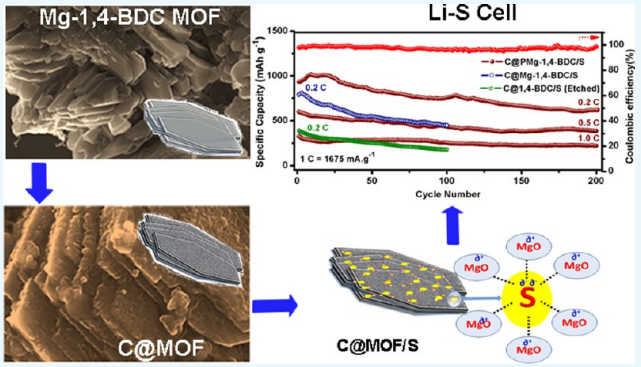

1. INTRODUCTION

Li−S battery is being projected as the most potential successor to the current Li-ion batteries, offering a theoretical specific capacity of 1675 mAh g^{-1} and a high energy density of 2500 Wh kg^{-1} owing to the reaction of Li and S involving transfer of $8e^-$ ($16Li + S_8 \leftrightarrow 8Li_2S$).[1] Recent research works on Li−S technology have led to significant advances; still, development of Li−S battery is plagued by two major obstacles: (1) intrinsically low electrical conductivity of S affecting the rate performance forcing a low active mass loading in the cathode[2] and (2) persistent dissolution of sulfide species from cathode into the electrolyte, leading to a "shuttle phenomenon", thereby reducing the Coulombic efficiency and cycling stability.[3] To overcome these obstacles, rational design of the cathode structure is required. In this respect, the importance of morphological architecture of the cathode support cannot be undermined. Carbon is the most widely used cathode support to host sulfur. One effective approach could be confining the sulfur species with advanced permanent porous structure of carbon derived from metal organic framework (MOF). MOF is a well-ordered framework constructed from the bonding between metal ions and polyfunctional organic ligands, resulting in a crystalline porous material with high surface area and tunable porosity.[4] MOFs are widely applied in heterogeneous catalysis,[5] gas storage and separation,[6] and drug delivery[7] for their ability to confine different substances, such as small molecules,[8] dyes,[9] drugs,[10] and metal nanoparticles.[11] MOF, by itself, can act as cathode support by confining S inside the pores as demonstrated by Tarascon et al.[12] with a mesoporous MIL-100 (Cr) MOF. However, due to their poor electronic and ionic conductivities and low electrochemical stability, the electrochemical performance of MOF/S cathodes[13] are still not comparable to carbon/S cathodes.[14−16] On the other hand, carbon derived from MOF could have the dual qualities of higher degree of S confinement and good electrical conductivity. Realizing this, recently, considerable research attention has been directed to fully explore the promises of carbon materials derived from MOF hosts for achieving superior battery performance.[17] MOFs have much more variable pore structures than other types of porous materials. Also, the pore and cage sizes and window apertures can be systematically tuned by varying different metal ions and ligands for confinement of sulfur. For example, it is found that cagelike pores can confine sulfur more efficiently than straight

Received: August 9, 2017
Accepted: September 28, 2017
Published: October 6, 2017

DOI: 10.1021/acsomega.7b01156
ACS Omega 2017, 2, 6481−6491

channels.[18,19] Moreover, the pore surfaces can be directly functionalized for further stronger interactions with sulfur. Also, it is possible that, even after carbonizing under high temperature, MOF-derived carbon could retain the morphology and porous structure of the parent MOF.[20] In addition to this, the metallic ions might be reduced to corresponding metal or metallic oxides that can act as "localized" inner templates to form mesopores[21] and simultaneously may enhance the electrical conductivity. Moreover, additional macropores could be formed during carbonization due to the synergic effect of organic material decomposition and gas activation, which would facilitate electrolyte access for transportation of ions. Therefore, to achieve high-performance carbon cathodes, the pore structures and properties of the parent MOFs need to be fully exploited. However, there are only a handful of reports available on MOF-derived carbon for Li−S battery application.[17,22−27]

Wu et al.[22] first reported the use of MOF-derived carbon for Li−S battery using zeolitic imidazolate framework (ZIF) material, ZIF-8 [$Zn(MeIM)_2$; MeIM = 2-methylimidazole], as the MOF precursor. Microporous carbon polyhedrons (MPCPs) obtained by carbonization in an inert gas at 1000 °C showed reversible capacity of about 420 mAh g^{-1} at current density of 100 mA g^{-1}, though with a low S loading of 43 wt %. Since then, several MOF-derived carbons have been studied mostly using ZIF as precursor. Li et al.[23] prepared tunable porous structure of carbon from ZIF-8, which delivered a high initial discharge capacity of ∼1500 mAh g^{-1}; however, it reduced to ∼800 mAh g^{-1} after 100 cycles. Xi et al.[17] used four sacrificial MOFs for the preparation of carbon: ZIF-8, MOF-519 (RT-MOF-5), solvothermally synthesized MOF-520 (solvo-MOF-5), and [$Zn_3(fumarate)_3(dmf)_2$] (Zn-fumarate). By melt−diffusion process, 55 wt % of sulfur could be encapsulated to the pyrolyzed carbon. Among these, carbon derived from Zn-fumarate MOF showed the best performance with an initial discharge capacity of 1471.8 mAh g^{-1}, which decayed quickly to 662.3 mAh g^{-1} after 40 cycles. Li et al.[24] developed nitrogen-doped carbon (NDC) spheres with abundant mesopores (22 nm) and micropores (0.5 nm) by carbonization of ZIF-8 MOF but could achieve sulfur loading of only 37%. The NDC−sulfur hybrid cathode exhibited a reversible capacity of 936.5 mAh g^{-1} at a current density of 335 mA g^{-1}. Bao et al.[25] designed a hierarchical architecture of multiwalled carbon nanotube@mesoporous carbon (MWCNT@Meso-C) using MWCNT@MOF-5, in which 58 wt % of S could be loaded by melt−diffusion method. The MWCNT@Meso-C/S sulfur cathode showed a high initial capacity of 1343 mAh g^{-1}, which gradually faded to 540 mAh g^{-1} after 50 cycles at 0.5 C. Yang et al.[26] synthesized French fry-like hierarchical porous carbon (FLHPC) with a one-dimensional structure from aluminum metal organic framework and achieved a relatively high S loading of 57 wt %. The S/FLHPC cathode showed a high initial discharge capacity of ∼1200 mA h g^{-1} at 0.1 C with a capacity retention of 68% at 0.5 C after 200 cycles. For improving the electrical conductivity, Li et al.[27] synthesized reduced graphene oxide (RGO)-wrapped cobalt-doped porous carbon polyhedron from ZIF-67 metal organic framework. The RGO−C−Co could accommodate ∼59 wt % of S and showed stable performance with a specific capacity of 949 mAh g^{-1} at the 300th cycle at a current density of 300 mA g^{-1}.

Motivated by these inspirational works, we have synthesized magnesium 1,4-benzenedicarboxylate MOF by a simple solvothermal method using poly(vinylpyrrolidone) (PVP) as a structure-directing agent as well as a precursor for preparing porous carbon with in situ embedment of Mg/MgO. Most of the MOFs used for deriving carbon are based on transition-metal ions, particularly Zn. Moving to a lighter metal, Mg would provide several advantages, such as low carbonization temperature. Also, 1,4-benzenedicarboxylic acid (1,4-BDC) is known to be a good organic connector to metal ions. The rigidity of its rodlike unit allows controlled growth of network structures.[28] Additionally, the conjugated carboxylate groups with an aromatic core having strong $\pi-\pi$ interaction can easily bond with metal ions forming thermodynamically driven highly ordered stable MOF structures.[29−31] However, compared to that on transition-metal−BDC MOFs, very little work is available on Mg-based MOF in general[32−34] and Mg−BDC MOF in particular.[28,35,36] MOFs intrinsically contain a large number of void spaces; also, there is poor orbital overlap with the metal ions due to the insulating nature of the organic ligands. As a result, the electrical conductivity of MOFs is generally low.[37,38] Carbonization at high temperatures would render the derived carbon still more porous due to escape of gas molecules. On the other hand, if some of the void spaces are filled with metal/metal oxide, there might be significant improvement in conductivity. Further, the embedded metal/metal oxide might help immobilization of S and also act as a catalyst for redox reaction between Li and S. With this aim, for the first time, we report the preparation and electrochemical properties of Mg/MgO-embedded carbon as Li−S battery cathode support derived from Mg−1,4-BDC MOF. We show that the simple strategy adopted here results in a better S confinement inside the cathode structure and a steady cycling behavior possibly due to suppression of S dissolution into the electrolyte and reduced polysulfide shuttle phenomenon.

2. RESULTS AND DISCUSSION

To check the formation of Mg−1,4-BDC MOF, powder X-ray diffraction (XRD) studies were carried out. Both the MOFs, synthesized with and without addition of PVP, exhibit sharp diffraction peaks, indicating a well-defined crystal structure (Figure 1a). The peak positions match well with the previously reported data for Mg−1,4-BDC MOF, indicating successful synthesis of the MOFs.[28] Noticeably, increase in sharpness and intensity of the peaks for PMg−1,4-BDC MOF suggests oriented growth, induced by PVP. Figure 1b shows the diffractograms for carbon derived from Mg−1,4-BDC MOF and PMg−1,4-BDC MOF. A broad hump at $2\theta \sim 26°$ indicates the presence of carbon, predominantly amorphous in nature. Additionally, five sharp peaks are observed at 2θ values of 36.88, 42.87, 62.24, 74.61, and 78.56°, all of which could be indexed to the cubic phase of MgO (JCPDS File No. 01-078-0430). Heat treatment of the parent MOFs at 800 °C in argon atmosphere generates carbon in situ from the organic moiety. Most of the Mg is evaporated because of having the lowest melting point (650 °C) among the alkaline earth metals, whereas a part is converted to MgO by reacting with the oxygen of the carboxylic group. However, the presence of any residual trace amount of Mg could not be confirmed as the strongest (011) peak for Mg is obscured by the (111) peak for MgO. No other impurity phase could be discerned. Therefore, the XRD results indicate successful synthesis of in situ MgO-incorporated MOF-derived carbon.

It is known that the carboxylate functional groups present in the organic ligand (benzene-1,4-dicarboxylate) can act as the

DOI: 10.1021/acsomega.7b01156
ACS Omega 2017, 2, 6481−6491

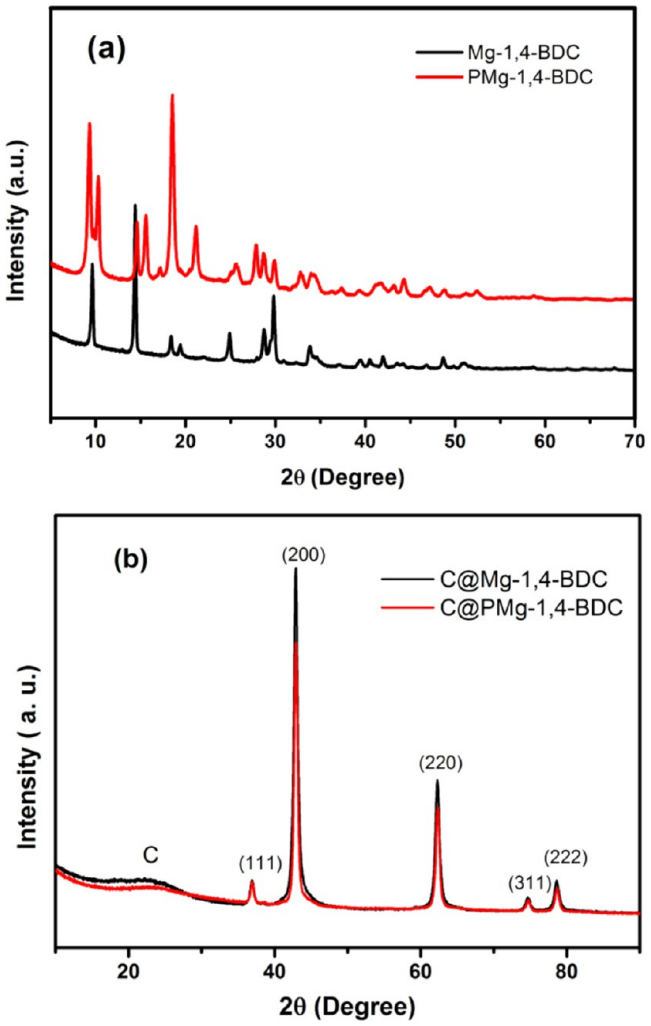

Figure 1. X-ray diffractograms of (a) Mg−1,4-BDC MOF and PMg−1,4-BDC MOF, synthesized with and without PVP assistance, respectively and (b) the corresponding derived carbons, C@Mg−1,4-BDC and C@PMg−1,4-BDC.

nucleation sites for the MOF crystal growth.[30,39] Here, PVP plays a crucial role during the solvothermal synthesis process as a structure-directing agent by regulating the growth and assembly of the unit structures and also acts as a stabilizing agent during the metal−ligand coordination.[40,41] The effect of PVP on the morphology is clearly manifested in the field emission scanning electron microscopy (FESEM) images of the synthesized MOFs (Figure 2). It is observed that the morphology of Mg−1,4-BDC MOF consists of small platelike particles assembled in a random fashion (Figure 2a), whereas large thick plates in orderly fashion are observed for PMg−1,4-BDC MOF (Figure 2c). Further, it is observed that in C@PMg−1,4-BDC (Figure 2d) the morphology of the parent MOF (PMg−1,4-BDC MOF) is transferred to the derived carbon, whereas in case of C@Mg−1,4-BDC (Figure 2b), irregular morphology consisting of thin sheets and particles is observed. However, due to the carbonization process, the surface of C@PMg−1,4-BDC becomes much rougher than the parent MOF. Transmission electron microscopy (TEM) images of C@PMg−1,4-BDC, shown in Figure 3, reveal a spongelike morphology with the presence of abundant pores extended in three dimensions forming zigzag channels resembling a maze. Large void spaces in such kind of spongelike carbon matrix will provide mechanical support to accommodate the strain induced by volume changes associated with the reaction of S with Li. Observation of diffused rings in the selected area diffraction (SAD) pattern (inset of Figure 3b) indicates the predominantly amorphous nature of the MOF-derived carbon. From Brunauer−Emmett−Teller (BET) measurements, a high surface area of 261.4 m^2 g^{-1} is obtained for C@PMg−1,4-BDC. The adsorption−desorption isotherms show a typical type IV isotherm with a hysteresis loop indicating the presence of mesoporous structures (Figure 4) and extending up to $P/P_0 \sim 1.0$. This distinct hysteresis loop appears before $P/P_0 = 0.8$ starting from $P/P_0 = 0.45$ (H1 type) and also at $P/P_0 \sim 0.8$−1.0 (H3 type), suggesting the existence of interconnected slit-type pores (originated from the pores of parent MOF) along with interparticle pores. In the pore size distribution plot, a bimodal distribution centered at ∼4 and ∼9 nm is found (inset of Figure 4) with a pore volume of 0.29 cc g^{-1}. Further, the narrow widths of pore size distribution peaks indicate uniformity of the mesoporous structures. The presence of abundant hierarchical pores and three-dimensionally connected zigzag mazelike channels would be beneficial for both electrolyte accessibility and retention of polysulfides within the carbon matrix. On the other hand, C@PMg−1,4-BDC shows a BET surface area of 310 m^2 g^{-1} and existence of larger pores of size ∼15 nm with a broad distribution in higher pore size range (macro region) with a pore volume of 0.77 cc g^{-1} (Figure S1, Supporting Information).

Raman spectral studies of the composites were undertaken for chemical characterization as well as for obtaining the structural information of the MOF-derived carbon. The presence of characteristic bands for graphitic carbon material can be observed from the Raman spectra of both the samples, C@Mg−1,4-BDC and C@PMg−1,4-BDC (Figure 5). The Raman active bands at ∼1348 (D band) and ∼1598 cm^{-1} (G band) with $I_D/I_G > 1$ revealed the formation of functionalized graphitic carbon with structural defects/disorder.[42−44] It is well known that D and G bands originated from the sp^2 graphitic carbon layer and defects are generated due to the formation sp^3 carbon within the lattice. The presence of a large number of structural defects ($I_D/I_G > 1$) would be beneficial to accommodate larger quantity of S by building a stronger interaction between carbon and sulfur, thereby strengthening the immobilization ability. Moreover, the presence of overtones of D band at ∼2900 cm^{-1} also suggests the formation of graphitic carbon material after heat treatment of the MOFs under inert atmosphere.[44] In addition to that, the broad low-intense peaks observed within the ranges of approximately 700−800 and 250−320 cm^{-1} can be assigned to the vibrational bands for Mg-O and Mg-OH, respectively.[45]

Surface chemical states of the elements are characterized by X-ray photoelectron spectroscopy (XPS) analysis of C@PMg−1,4-BDC. The surface survey scan shows the presence of C 1s along with O 1s and Mg 2p (Figure S2, Supporting Information). Deconvolution of high-resolution C 1s spectra (Figure 6a) indicates the presence of several surface functional groups.[46,47] The peaks at 284.45 and 284.82 eV correspond to the skeletal C=C and C−C of graphitic carbon material, respectively, and the corresponding $\pi-\pi^*$ binding energy is observed at 290.90 eV.[42,46,48] High-resolution XPS images of O 1s (Figure 6b) reveal the presence of MgO and $Mg(OH)_2$ as the main chemical states of oxygen-containing Mg moieties. Interestingly, the presence of mixed hydrated forms of Mg along with metallic Mg is confirmed from the deconvoluted Mg

DOI: 10.1021/acsomega.7b01156
ACS Omega 2017, 2, 6481−6491

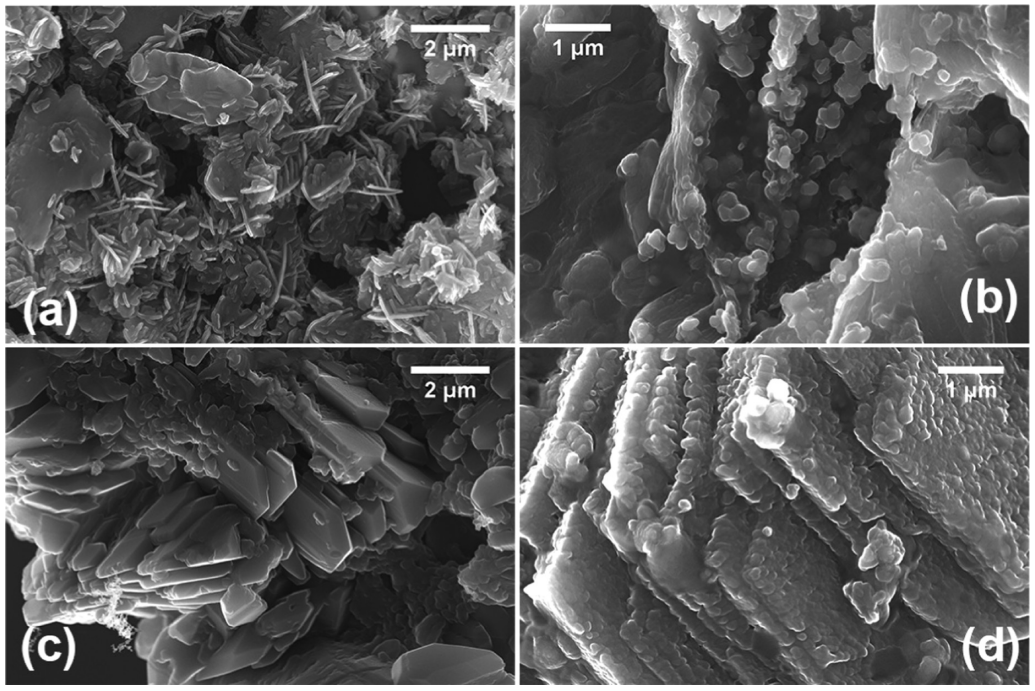

Figure 2. FESEM images of (a) Mg−1,4-BDC MOF, (b) C@Mg−1,4-BDC, (c) PMg−1,4-BDC MOF, and (d) C@PMg−1,4-BDC.

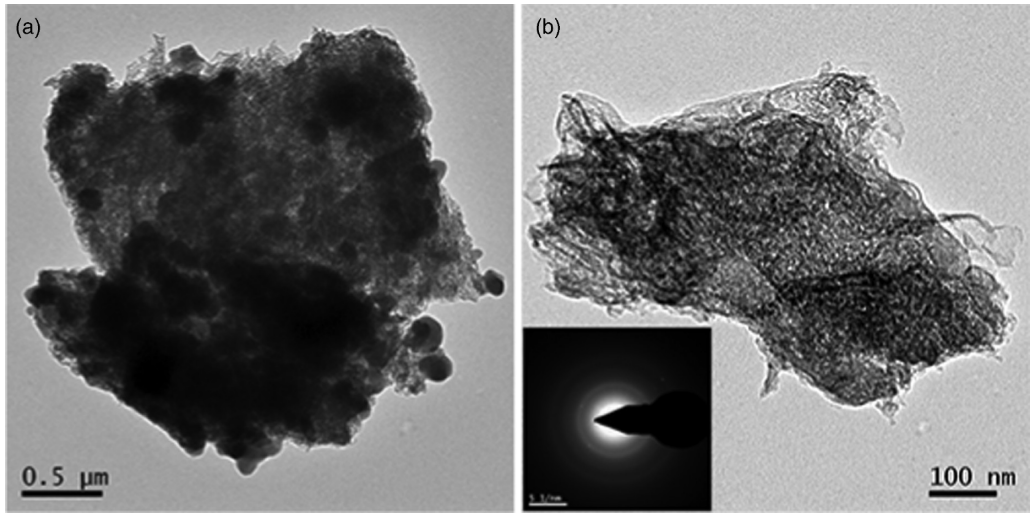

Figure 3. (a, b) TEM images of C@PMg−1,4-BDC at different magnifications. The SAD pattern is given in the inset of (b).

2p spectra (Figure 6c).[48,49] Notably, the presence of a minute amount of metallic Mg would significantly increase the electrical conductivity of the carbon host, thus facilitating the charge transfer during the redox processes.

C@Mg−1,4-BDC/S and C@PMg−1,4-BDC/S cathodes have been prepared by infiltrating sulfur into the respective MOF-derived carbon by CS_2 route. The X-ray diffractogram of C@PMg−1,4-BDC/S (Figure S3, Supporting Information) is in conformation to JCPDS File No. 01-083-2283 and indicates the presence of sulfur predominantly in S_8 form. The sulfur content in the respective MOF-derived C/S composites has been determined by the weight losses of C@Mg−1,4-BDC/S and C@PMg−1,4-BDC/S by thermogravimetric analysis (TGA) in air (Figure S4, Supporting Information). Both the composites exhibit nearly identical TGA profiles from which a high degree of sulfur loading of 69.1 wt % could be determined. The relative composition of the composites is estimated to be S 69.1 wt % (62.7 mol %), C 8.9 wt % (21.5 mol %), and MgO 22.0 wt % (15.8 mol %). Electrochemical performances of carbon host materials are usually compromised by low sulfur loading ability, typically in the range of 40−60 wt %,[50−52] which greatly reduces the overall energy density of Li−S cells. In the present case, such high S loading might have resulted from the hierarchical mesoporous structure of carbon with bimodal pore size producing a capillary effect, the presence of MgO with surface affinity toward electronegative S, and a large number of structural defects, which would promote a stronger interaction between carbon and sulfur, thereby strengthening the immobilization ability. Energy-dispersive X-ray (EDX) spectrum and elemental distribution map of C@PMg−1,4-BDC/S (Figures S5 and S6, Supporting Information) indicate a homogeneous distribution of C, O, Mg, and S in the composite cathode.

DOI: 10.1021/acsomega.7b01156
ACS Omega 2017, 2, 6481−6491

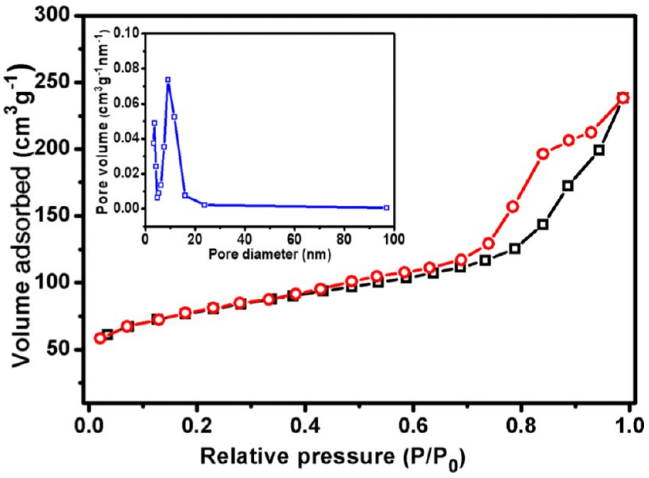

Figure 4. Nitrogen gas adsorption−desorption isotherms for C@PMg−1,4-BDC. The inset shows the pore size distribution.

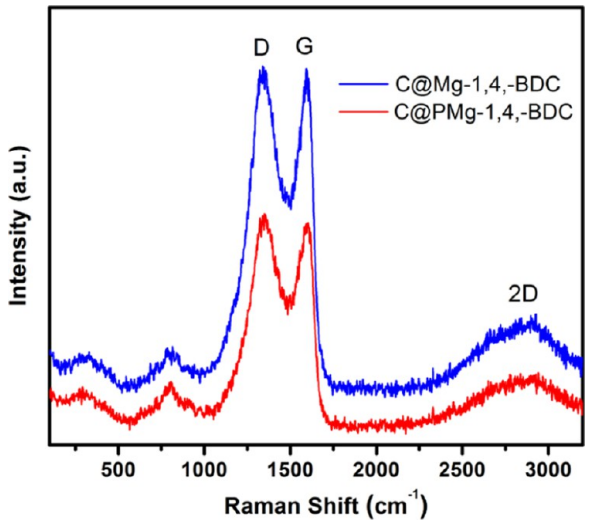

Figure 5. Raman spectra of C@Mg−1,4-BDC and C@PMg−1,4-BDC.

The electrochemical properties of the developed C@Mg−1,4-BDC/S and C@PMg−1,4-BDC/S cathodes were first examined by cyclic voltammetry (CV) in the potential window of 1.5−3.0 V (Figure 7a,b). Two well-defined cathodic peaks at ∼2.36 and ∼2.06 V in the cyclic voltammograms are observed due to multistep reduction of sulfur[53] and could be assigned in the following way: the broad reduction peak at around 2.36 V corresponds to the redox reaction of elemental S_8 ring and the formation of polysulfides (S_8^{2-}), whereas the peak at ∼2.06 V reflects the deep redox reaction from higher polysulfide species (Li_2S_n, $4 < n < 8$) to the lower polysulfide species (Li_2S_n, $n \leq 2$). During the first anodic scan, two typical oxidation peaks were observed, at ∼2.43 and ∼2.55 V, where the insoluble Li_2S changed into polysulfides and eventually to elemental S_8 form. During the subsequent scans, it was found that the cathodic peaks and the first anodic peak shift only marginally, but the higher oxidation peak in the anodic scan shifts ∼0.15 V to the higher potential side (at ∼2.7 V). Such shifting of peak position could be assigned to the so-called electrode activation process, that is, rearrangement of orthogonal sulfur from the original site to a more stable site.[53−55] The peak positions in the subsequent

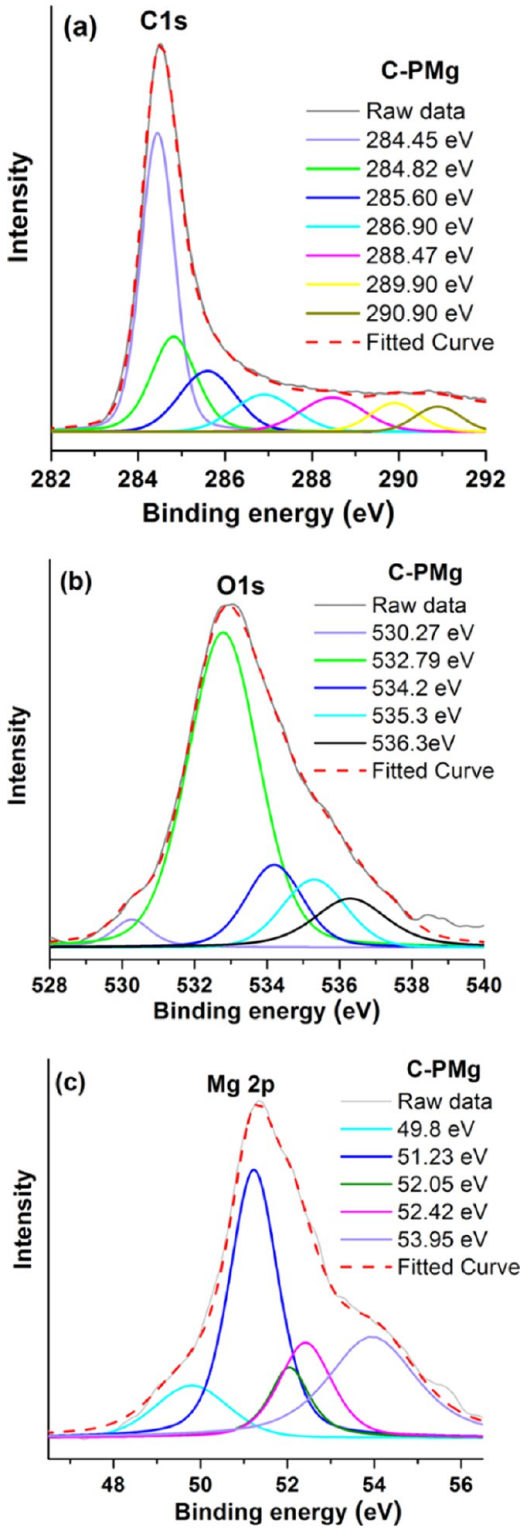

Figure 6. High-resolution XPS images of C@PMg−1,4-BDC: (a) C 1s, (b) O 1s, and (c) Mg 2p.

cycles remain nearly unchanged, implying good reversibility.[56,57]

The initial galvanostatic charge−discharge behaviors of C@Mg−1,4-BDC/S and C@PMg−1,4-BDC/S cathodes were evaluated at a current rate of 0.02 C (1 C = 1675 mA g^{-1}) in the potential window of 1.5−2.8 V versus Li^+/Li (Figure 8a,b). Two flat discharge plateaus located at 2.36 and 2.06 V

DOI: 10.1021/acsomega.7b01156
ACS Omega 2017, 2, 6481−6491

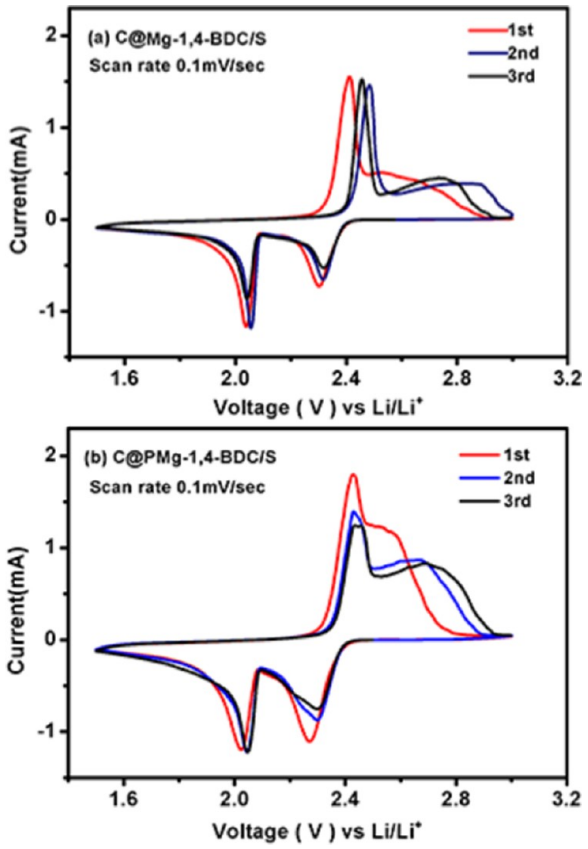

Figure 7. First three successive cyclic voltammograms for (a) C@Mg−1,4-BDC/S and (b) C@PMg−1,4-BDC/S in the potential window of 1.5−3.0 V at a sweep rate of 0.1 mV s^{-1}.

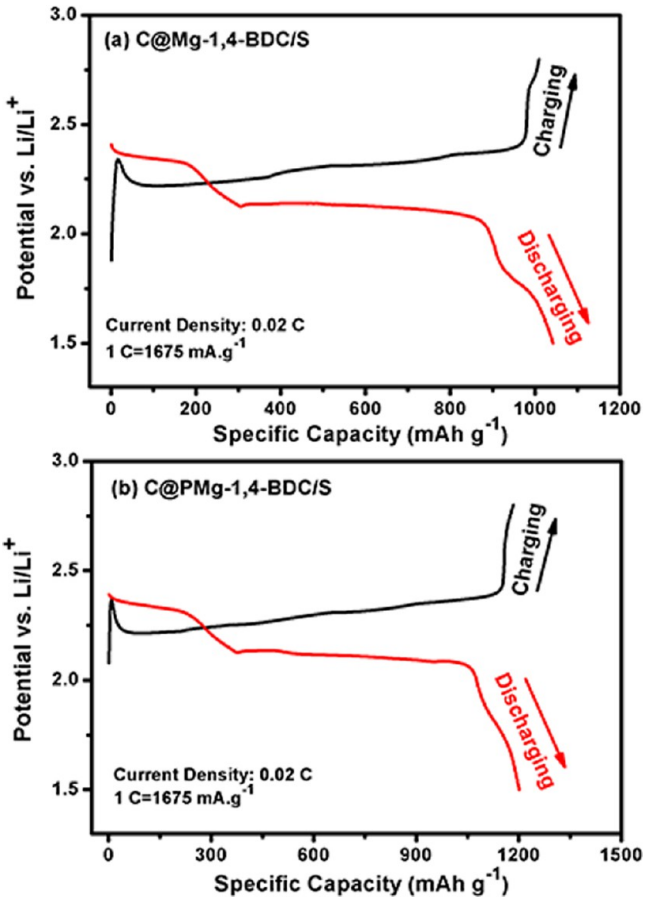

Figure 8. Initial discharge−charge profiles of (a) C@Mg−1,4-BDC/S and (b) C@PMg−1,4-BDC/S

were clearly observed, which are in good agreement with the CV results. The initial discharge/charge capacities of 1041/1009 and 1201/1184 mAh g^{-1} were obtained for C@Mg−1,4-BDC/S and C@PMg−1,4-BDC/S, respectively, with corresponding very high first-cycle Coulombic efficiencies of 96.9 and 98.6%.

Cycling performances of C@Mg−1,4-BDC/S and C@PMg−1,4-BDC/S composite were compared at a current rate of 0.2 C (Figure 9). C@PMg−1,4-BDC/S shows a capacity of 935 mAh g^{-1} at the first cycle, which reduces to 757 mAh g^{-1} (81% retention) after 100 cycles and to 621 mAh g^{-1} after 200 cycles (66.4% retention). It is possible that $LiNO_3$ additive in the electrolyte could decompose at potentials <1.6 V, but no definite signature was observed in cyclic voltammogram. Also, galvanostatic charge−discharge (GCD) profiles at different cycling intervals indicate a small plateau only at the first cycle, which is not observed in subsequent cycles (Figure S7, Supporting Information). Moreover, because the reduction products, if any, formed at potentials >1.5 V are soluble in the electrolyte, they do not significantly affect the cycling and capacity retention as observed by others.[58] Despite having a high S loading of 69.1 wt %, the observed capacity values for C@PMg−1,4-BDC/S are comparable to or higher than those MOF-derived carbon materials (a detailed performance comparison of different carbon materials derived from MOF (C@MOF) is given in Table S1, Supporting Information).[17,21−27,50,51,59] On the other hand, C@Mg−1,4-BDC/S shows a relatively lower capacity of 791 mAh g^{-1} at the first cycle at the same current rate and retains only 56.6% of capacity (448 mAh g^{-1}) after 100 cycles (Figure 9). These results demonstrate that the morphological advantages in C@PMg−1,4-BDC/S resulted in a greater capacity. It is believed that the abundant channelized mesopores with narrow sizes (4 and 9 nm) facilitate easy access to as well as diffusion of electrolyte and concurrently immobilize S by cohesive force due to capillary effect. Also, the mazelike zigzag channels would be more effective for confinement of polysulfides than straight channels.[18,19] To see the effect of Mg/MgO embedded in the carbon matrix, a control sample was prepared by removing Mg/MgO from C@Mg−1,4-BDC by acid treatment. Cycling data of the control sample C@1,4-BDC/S at 0.2 C rate show much inferior performance (392 mAh g^{-1}, 46% retention after 100 cycles) to either C@Mg−1,4-BDC/S or C@PMg−1,4-BDC/S, confirming the positive effect of Mg/MgO. It is probable that the presence of Mg would enhance the charge transport, whereas the presence of MgO might help in the confinement of S species within the cathode structure through strong interaction with S for surface polarity compensation. This is quite likely for materials with a high affinity toward electronegative atoms, such as MgO, where even nonpolar termination may readily develop ad-layer.[60,61]

To explain the superior cycling performance of C@PMg−1,4-BDC/S, a detailed XPS analysis was carried out to verify whether any interaction present between Mg and S in this sample. The surface survey scan shows the presence of S 2p binding energy peak along with C 1s, O 1s, and Mg 2p (Figure S8, Supporting Information). Further, deconvolution of high-resolution S 2p and Mg 2p binding energy peaks was carried out to understand the interaction between these elements. In

DOI: 10.1021/acsomega.7b01156
ACS Omega 2017, 2, 6481−6491

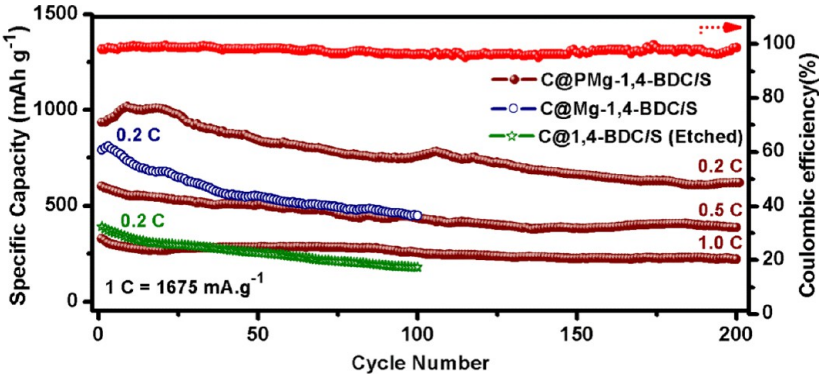

Figure 9. Cycling performance of C@1,4-BDC/S-etched (without embedded Mg/MgO) and C@Mg−1,4-BDC/S at 0.2 C and C@PMg−1,4-BDC/S at 0.2, 0.5, and 1 C.

high-resolution S 2p XPS images (Figure 10a), S $2p_{3/2}$ and S $2p_{1/2}$ doublet appears at binding energy values of 163.89 and

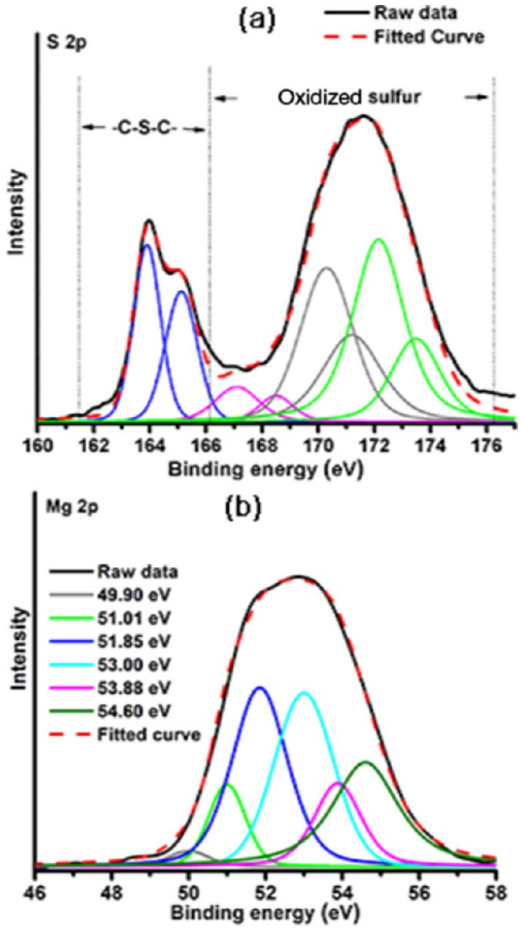

Figure 10. High-resolution XPS images of C@PMg−1,4-BDC/S: (a) S 2p and (b) Mg 2p.

165.15 eV corresponding to the C−S and C═S bonds that subsequently reveal the incorporation of sulfur into the graphitic carbonaceous framework.[61] Other peaks in the higher binding energy region of 167−174 eV can be assigned to the oxidized forms of sulfur.[62−64] Deconvolution of high-resolution Mg 2p spectrum also gives some interesting observations. The binding energy peaks related to the oxygen-containing Mg moieties (Figure 10b) get shifted toward higher-energy region compared to those observed for C@PMg−1,4-BDC (Figure 6c). Additionally, the relative intensity of the peak corresponding to the free metallic Mg (49.90 eV) gets reduced and simultaneously a new peak has developed at 51.01 eV, which corresponds to the metallic Mg engaged in the interaction with sulfur.[65] Thus, XPS study clearly indicates the presence of chemical interactions between Mg and the sulfur component present in the hybrid system. Thereby, the dissolution of polysulfide into the electrolyte, which is the main cause for the "shuttle phenomenon" and the consequent capacity fading, is restricted to a great extent.[65,66] Further, to check the rate capability and electrochemical stability, cycling of C@PMg−1,4-BDC/S composite was carried out at current rates of 0.5 and 1 C for 200 cycles (Figure 9). Reversible capacities of 386 and 220 mAh g^{-1} were obtained at 0.5 and 1.0 C, respectively, with retentions of 65 and 67% after 200 cycles. Also, the Coulombic efficiency (at 1 C rate) is found to be quite high (∼98%) even at the 200th cycle (Figure 9). Therefore, the developed C@PMg−1,4-BDC/S cathode shows good cycling stability. To investigate any morphological changes upon cycling, ex situ FESEM study was undertaken on the C@PMg−1,4-BDC/S electrode after 100 cycles at 0.2 C rate. It is observed that even after prolonged cycling the general sheetlike morphology of C@PMg−1,4-BDC is preserved, although the sheets appear somewhat fluffy due to infiltrated S within the carbon matrix (Figure S9, Supporting Information).

Electrochemical impedance spectroscopy (EIS) provides useful insight into the degradation mechanism of the cell. A systematic study was undertaken by recording the impedance spectra of C@PMg−1,4-BDC/S at different cycling intervals at 0.2 C rate, and the Nyquist plots are shown in Figure 11. The as-assembled cell shows a low solution resistance (R_s) of 2.3 Ω. Upon cycling, the increase in R_s is only marginal with values of 3.2, 3.7, and 4.2 Ω after the 1st, 50th, and 100th cycles, respectively. This indicates that S is confined to the cathode structure with no significant dissolution into the electrolyte. The charge-transfer resistance (R_{ct}) of the as-assembled cell is found to be 92 Ω. The R_{ct} gradually decreases with cycling up to about 50 cycles and thereafter remains constant with a value of about 20 Ω. The decrease in R_{ct} can be attributed to the gradual wetting of the electrodes and activation of the pores.[67] This also explains a slight increase and then decrease of capacity for about 50 cycles during the cycling test.

DOI: 10.1021/acsomega.7b01156
ACS Omega 2017, 2, 6481−6491

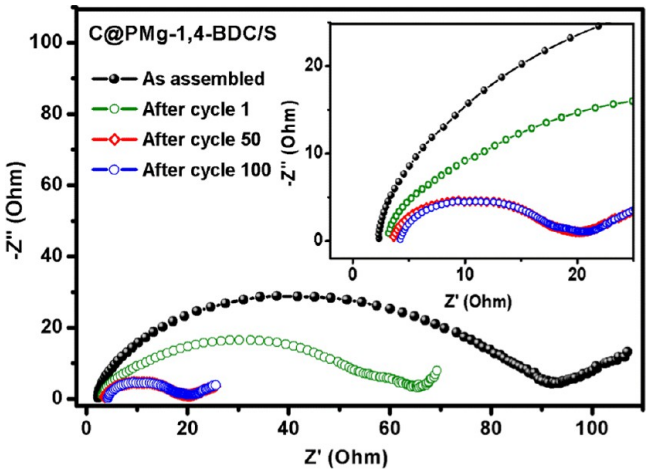

Figure 11. Nyquist plots of C@PMg−1,4-BDC/S at different cycling intervals at 0.2 C. The inset shows a zoomed view in the high frequency region.

3. CONCLUSIONS

In summary, we report the preparation and electrochemical properties of Mg/MgO-embedded carbon as Li−S battery cathode support derived from Mg−1,4-BDC MOF. The derived carbon mimics the hexagonal sheetlike morphology of the parent MOF having a high surface area of 310 m^2 g^{-1}. The MOF-derived carbon contains abundant mesopores with bimodal pore size distributions of ∼4 and ∼9 nm, which are channelized in three dimensions in a zigzag way resembling a maze. The presence of structural defects/disorder and mazelike pores helps immobilization of sulfur within the cathode structure through capillary forces. Additionally, it is found that embedded MgO further supports confinement of sulfur species through chemical interactions between Mg and sulfur, limiting the polysulfide shuttle phenomenon during redox reactions, whereas metallic Mg enhances the electrical conductivity. High sulfur loading (69.1 wt %), good reversible capacity (1184 mAh g^{-1}), and electrochemical cycling stability have been achieved, highlighting the efficacy of the presently designed cathode support for efficient confinement of polysulfides.

4. EXPERIMENTAL SECTION

4.1. Material Synthesis. *4.1.1. Synthesis of Mg−1,4-BDC MOF and PVP-Assisted Mg−1,4-BDC MOF.* In a typical procedure for the synthesis of PVP-assisted Mg−1,4-BDC MOF, 0.33 g (2 mmol) of benzene-1,4-dicarboxylic acid (BDC) (98%; Sigma-Aldrich) was dissolved in 20 mL of dimethylformamide (DMF) (≥99%; Sigma-Aldrich) and 2.32 g of PVP (MW 58 000; Alfa Aesar) was added to the BDC solution. A separate solution was prepared by dissolving 0.6 g (4 mmol) of $Mg(NO_3)_2{\cdot}6H_2O$ (99%; Sigma-Aldrich) in 20 mL of DMF. The two solutions were mixed dropwise under stirring condition and kept for 5 min. The resulting mixture was transferred into a 100 mL Teflon autoclave and heated at 160 °C for 48 h. After cooling to room temperature, the yellowish powder was washed repeatedly with ethanol to wash out residual PVP and dried. The synthesized MOF powder was named as PMg−1,4-BDC MOF.

For preparation of Mg−1,4-BDC MOF without PVP assistance, the same procedure was followed except for the addition of PVP into the precursor BDC solution. This sample was named as Mg−1,4-BDC MOF.

4.1.2. Synthesis of MOF-Derived Carbon (C@Mg−1,4-BDC, C@PMg−1,4-BDC, and C@1,4-BDC). Mg−1,4-BDC MOF was put into a ceramic boat and heated at 800 °C for 3 h in an Ar-filled tubular furnace at a heating rate of 5 °C min^{-1}. The resulting black flocculent powder was labeled as C@Mg−1,4-BDC.

In similar way, PMg−1,4-BDC MOF was carbonized to obtain C@PMg−1,4-BDC.

For comparison purpose, embedded Mg/MgO is removed from the carbon structure by etching C@Mg−1,4-BDC using hydrofluoric acid (≥99.99%; Sigma-Aldrich). The sample is named as C@1,4-BDC.

4.1.3. Synthesis of MOF-Derived Carbon/S Composites (C@Mg−1,4-BDC/S, C@PMg−1,4-BDC/S, and C@1,4-BDC/S). C@Mg−1,4-BDC (0.2 g) and commercial sulfur (0.6 g, ≥99.5%; Sigma-Aldrich) were dispersed into 6 mL of CS_2. The mixture was stirred at room temperature until the solvent was evaporated completely. It was then subjected to heat treatment in Ar atmosphere in two steps: at 155 °C for 12 h, followed by 200 °C for 2 h. The obtained powder was named as C@Mg−1,4-BDC/S. In similar way, C@PMg−1,4-BDC/S and C@1,4-BDC/S were prepared from C@PMg−1,4-BDC and C@1,4-BDC, respectively.

4.2. Material Characterization. To examine the formation of MOFs and phase purity of the derived carbon, X-ray powder diffraction studies were carried out. X-ray diffractograms were recorded in the 2θ range of 5−70° at a scanning rate of 2° min^{-1} by a Rigaku SmartLab X-ray diffractometer operating at 9 kW (200 mA; 45 kV) using Cu Kα radiation. Microstructure and morphology of the MOFs and the derived carbon were examined by a field emission scanning electron microscope (Zeiss Supra 35, Germany). Thermogravimetric analyses (TGA) of the powder samples were carried out under argon flow in the temperature range of 27−800 °C at a heating rate of 5 °C min^{-1} using simultaneous thermal analyzer (STA 449F; Netzsch, Germany). Brunauer−Emmett−Teller (BET) surface area measurements were carried out by N_2 gas adsorption at 77.3 K using a Quantachrome Autosorb surface analyzer. Pore size distribution was calculated from the sorption isotherm by the Barrett−Joyner−Halenda method. Raman signals were obtained from powder samples using a Renishaw InVia micro-Raman spectrometer with excitation of argon-ion (514 nm) lasers with a resolution of 1 cm^{-1}. The laser power was kept sufficiently low to avoid local heating of the sample. X-ray photoelectron spectroscopy (XPS) measurements of MOF-derived carbon were done on a PHI 5000 VersaProbe II XPS system with Al Kα source and a charge neutralizer at room temperature, maintaining a base pressure of about 6×10^{-10} mbar and energy resolution of 0.6 eV.

4.3. Electrochemical Characterization. *4.3.1. Cathode Preparation.* MOF-derived C/S composite cathodes were fabricated by the standard slurry casting method. The slurry was made by intimately mixing the prepared MOF-derived C/S composite, Super-P (conducting agent), and poly(vinylidene fluoride) (binder) in a weight ratio of 80:10:10 in *n*-methyl pyrrolidinone as solvent. The slurry was coated onto Al foil (thickness, 19 μm) and dried at 60 °C under vacuum overnight. After calendaring and roll pressing of the resulting film, circular disks of diameter 15 mm were cut and used as electrode. The active mass loading was typically ∼2 mg cm^{-2}.

DOI: 10.1021/acsomega.7b01156
ACS Omega 2017, 2, 6481−6491

4.3.2. Cell Fabrication. The electrochemical properties were evaluated by fabricating 2032-type coin cells in an argon-filled glovebox (M′BRAUN, Germany), where the moisture and oxygen levels were kept at <0.5 ppm. Li metal was used as the counter electrode as well as the reference electrode, Celgard 2300 was used as the separator, and the electrolyte was 1 M lithium bis(trifluoromethane)sulfonimide (LiTFSI, ≥98%; Alfa Aesar) and 0.1 M lithium nitrate ($LiNO_3$, ≥99%; Acros Organics) dissolved in a mixture of 1,3-dioxolane (99.8%; Acros Organics) and 1,2-dimethoxyethane (≥99%; Acros Organics) (1:1 vol %).

4.3.3. Electrochemical Measurements. Cyclic voltammetry (CV) was carried out in the potential window of 1.5−3.0 V using a galvanostat−potentiostat (PGSTAT302N; Autolab, the Netherlands). Electrochemical impedance spectroscopy (EIS) experiments were also performed using the same galvanostat−potentiostat in the frequency range of 100 kHz to 0.1 Hz. Galvanostatic charge−discharge measurements were carried out in the potential window of 1.5−2.8 V using an automatic battery tester (BT2000; Arbin).

■ ASSOCIATED CONTENT

Supporting Information

The Supporting Information is available free of charge on the ACS Publications website at DOI: 10.1021/acsomega.7b01156.

Nitrogen gas adsorption−desorption isotherms for C@Mg−1,4-BDC (Figure S1); XPS survey scans of C@PMg−1,4-BDC and C@PMg−1,4-BDC/S (Figure S2 and Figure S8); X-ray diffractogram of C@PMg−1,4-BDC/S composite and simulated pattern for S_8 (Figure S3); TGA of C@Mg−1,4-BDC/S and C@PMg−1,4-BDC/S (Figure S4); EDX of C@PMg−1,4-BDC/S& elemental distribution in C@PMg−1,4-BDC/S (Figure S5 and Figure S6); GCD profiles of C@PMg−1,4-BDC/S at different cycling intervals (Figure S7); FESEM of C@PMg−1,4-BDC/S electrode after 100 cycles (Figure S9); electrochemical performance comparison of different MOF-derived carbon materials (Table S1) (PDF)

■ AUTHOR INFORMATION

Corresponding Authors

*E-mail: gde@cgcri.res.in (G.D.).
*E-mail: mahanty@cgcri.res.in (S.M.).

ORCID

Goutam De: 0000-0003-0271-1634
Sourindra Mahanty: 0000-0002-4229-7135

Author Contributions

The manuscript was written through contributions of all authors.

Notes

The authors declare no competing financial interest.

■ ACKNOWLEDGMENTS

Financial support from SERB, DST India vide project number EMR/2014/000729 is gratefully acknowledged. S.C. thanks UGC for fellowship.

■ REFERENCES

(1) Yang, Y.; Zheng, G.; Cui, Y. Nanostructured sulfur cathodes. *Chem. Soc. Rev.* **2013**, *42*, 3018−3032.

(2) Zhou, W.; Chen, H.; Yu, Y.; Wang, D.; Cui, Z.; DiSalvo, F. J.; Abruña, H. D. Amylopectin wrapped graphene oxide/sulfur for improved cyclability of lithium sulfur battery. *ACS Nano* **2013**, *7*, 8801−8808.

(3) Bresser, D.; Passerini, S.; Scrosati, B. Recent progress and remaining challenges in sulfur-based lithium secondary batteries − a review. *Chem. Commun.* **2013**, *49*, 10545−10562.

(4) Song, L.; Zhang, J.; Sun, L.; Xu, F.; Zhang, H.; Si, X.; Jiao, C.; Li, Z.; Liu, S.; Liu, Y.; Zhou, H.; Sun, D.; Du, Y.; Cao, Z.; Gabelica, Z.; et al. Mesoporous metal−organic frameworks: design and applications. *Energy Environ. Sci.* **2012**, *5*, 7508−7520.

(5) Yadav, M.; Xu, Q. Catalytic chromium reduction using formic acid and metal nanoparticles immobilized in a metal−organic framework. *Chem. Commun.* **2013**, *49*, 3327−3329.

(6) Zhou, W. Methane storage in porous metal−organic frameworks: current records and future perspectives. *Chem. Rec.* **2010**, *10*, 200−204.

(7) An, J.; Geib, S. J.; Rosi, N. L. Cation-triggered drug release from a porous zinc−adeninate metal−organic framework. *J. Am. Chem. Soc.* **2009**, *131*, 8376−8377.

(8) Xiang, S.; Zhou, W.; Zhang, Z.; Green, M. A.; Liu, Y.; Chen, B. Open Metal Sites within Isostructural Metal−Organic Frameworks for Differential Recognition of Acetylene and Extraordinarily High Acetylene Storage Capacity at Room Temperature. *Angew. Chem., Int. Ed.* **2010**, *49*, 4615−4618.

(9) Yu, J.; Cui, Y.; Wu, C.; Yang; Wang, Z.; O'Keeffe, M.; Chen, B.; Qian, G. Second-order nonlinear optical activity induced by ordered dipolar chromophores confined in the pores of an anionic metal−organic framework. *Angew. Chem., Int. Ed.* **2012**, *51*, 10542−10545.

(10) Liu, B.; Li, H.; Xu, X.; Li, X.; Lv, N.; Singh, V.; Stoddart, J. F.; York, P.; Xu, X.; Gref, R.; Zhang, J. Optimized synthesis and crystalline stability of γ-cyclodextrin metal−organic frameworks for drug adsorption. *Int. J. Pharm.* **2016**, *514*, 212−219.

(11) Hermes, S.; Schröter, M.-K.; Schmid, R.; Khodeir, L.; Muhler, M.; Tissler, A.; Fischer, R. W.; Fischer, R. A. Metal@MOF: Loading of highly porous coordination polymers host lattices by metal organic chemical vapor deposition. *Angew. Chem., Int. Ed.* **2005**, *44*, 6237.

(12) Demir-Cakan, R.; Morcrette, M.; Nouar, F.; Davoisne, C.; Devic, T.; Gonbeau, D.; Dominko, R.; Serre, C.; Férey, G.; Tarascon, J.-M. Cathode composites for Li−S batteries via the use of oxygenated porous architectures. *J. Am. Chem. Soc.* **2011**, *133*, 16154−16160.

(13) Bao, W.; Zhang, Z.; Qu, Y.; Zhou, C.; Wang, X.; Li, J. Confine sulfur in mesoporous metal−organic framework @ reduced graphene oxide for lithium sulfur battery. *J. Alloys Compd.* **2014**, *582*, 334−340.

(14) Wang, H.; Zhang, C.; Chen, Z.; Liu, H. K.; Guo, Z. Large-scale synthesis of ordered mesoporous carbon fiber and its application as cathode material for lithium−sulfur batteries. *Carbon* **2015**, *81*, 782−787.

(15) Peng, H.-J.; Huang, J.-Q.; Zhao, M.-Q.; Zhang, Q.; Cheng, X.-B.; Liu, X.-Y.; Qian, W.-Z.; Wei, F. Nanoarchitectured graphene/CNT@porous carbon with extraordinary electrical conductivity and interconnected micro/mesopores for lithium−sulfur batteries. *Adv. Funct. Mater.* **2014**, *24*, 2772−2781.

(16) Wang, Z.; Li, X.; Cui, Y.; Yang, Y.; Pan, H.; Wang, Z.; Wu, C.; Chen, B.; Qian, G. Metal−organic framework with open metal sites for enhanced confinement of sulfur and lithium−sulfur battery of long cycling life. *Cryst. Growth Des.* **2013**, *13*, 5116−5120.

(17) Xi, K.; Cao, S.; Peng, X.; Ducati, C.; Kumar, R. V.; Cheetham, A. K. Carbon with hierarchical pores from carbonized metal−organic frameworks for lithium sulphur batteries. *Chem. Commun.* **2013**, *49*, 2192−2194.

(18) Wang, Z.; Dou, Z.; Cui, Y.; Yang, Y.; Wang, Z.; Qian, G. Sulfur encapsulated ZIF-8 as cathode material for lithium−sulfur battery with improved cycleability. *Microporous Mesoporous Mater.* **2014**, *185*, 92−96.

(19) Zhou, J.; Li, R.; Fan, X.; Chen, Y.; Han, R.; Li, W.; Zheng, J.; Wang, B.; Li, X. Rational design of a metal−organic framework host for sulfur storage in fast, long-cycle Li−S batteries. *Energy Environ. Sci.* **2014**, *7*, 2715−2724.

DOI: 10.1021/acsomega.7b01156
ACS Omega 2017, 2, 6481−6491

(20) Yang, S. J.; Antonietti, M.; Fechler, N. Self-Assembly of metal phenolic mesocrystals and morphosynthetic transformation toward hierarchically porous carbons. *J. Am. Chem. Soc.* **2015**, *137*, 8269−8273.
(21) Yang, X.; Yu, Y.; Yan, N.; Zhang, H.; Li, X.; Zhang, H. 1-D oriented cross-linking hierarchical porous carbon fibers as a sulfur immobilizer for high performance lithium−sulfur batteries. *J. Mater. Chem. A* **2016**, *4*, 5965−5972.
(22) Wu, H. B.; Wei, S.; Zhang, L.; Xu, R.; Hng, H. H.; Lou, X. W. D. Embedding sulfur in MOF-derived microporous carbon polyhedrons for lithium−sulfur batteries. *Chem. − Eur. J.* **2013**, *19*, 10804−10808.
(23) Li, X.; Sun, Q.; Liu, J.; Xiao, B.; Li, R.; Sun, X. Tunable porous structure of metal organic framework derived carbon and the application in lithium sulfur batteries. *J. Power Sources* **2016**, *302*, 174−179.
(24) Li, Z.; Yin, L. Nitrogen-doped MOF-derived micropores carbon as immobilizer for small sulfur molecules as a cathode for lithium sulfur batteries with excellent electrochemical performance. *ACS Appl. Mater. Interfaces* **2015**, *7*, 4029−4038.
(25) Bao, W.; Zhang, Z.; Zhou, C.; Lai, Y.; Li, J. Multi-walled carbon nanotubes @ mesoporous carbon hybrid nanocomposites from carbonized multi-walled carbon nanotubes @ metaleorganic framework for lithium sulfur battery. *J. Power Sources* **2014**, *248*, 570−576.
(26) Yang, X.; Yan, N.; Zhou, W.; Zhang, H.; Li, X.; Zhang, H. Sulfur embedded in one-dimensional French fries like hierarchical porous carbon derived from a metal−organic framework for high performance lithium−sulfur batteries. *J. Mater. Chem. A* **2015**, *3*, 15314−15323.
(27) Li, Z.; Li, C.; Ge, X.; Ma, J.; Zhang, Z.; Li, Q.; Wang, C.; Yin, L. Reduced graphene oxide wrapped MOFs-derived cobalt-doped porous carbon polyhedrons as sulfur immobilizers as cathodes for high performance lithium sulfur batteries. *Nano Energy* **2016**, *23*, 15−26.
(28) Davies, R. P.; Less, R. J.; Lickiss, P. D.; White, A. J. P. Framework materials assembled from magnesium carboxylate building units. *Dalton Trans.* **2007**, 2528−2535.
(29) Maiti, S.; Pramanik, A.; Manju, U.; Mahanty, S. Cu_3(1,3,5-benzenetricarboxylate)$_2$ metal−organic framework: a promising anode material for lithium-ion battery. *Microporous Mesoporous Mater.* **2016**, *226*, 353−359.
(30) Maiti, S.; Pramanik, A.; Manju, U.; Mahanty, S. Reversible lithium storage in manganese 1,3,5-benzenetricarboxylate metal−organic framework with high capacity and rate performance. *ACS Appl. Mater. Interfaces* **2015**, *7*, 16357−16363.
(31) Wang, M.; Xu, X.; Liu, Y.; Li, Y.; Lu, T.; Pan, L. From metal−organic frameworks to porous carbons: a promising strategy to prepare high-performance electrode materials for capacitive deionization. *Carbon* **2016**, *108*, 433−439.
(32) Dincă, M.; Long, J. R. Strong H_2 binding and selective gas adsorption within the microporous coordination solid $Mg_3(O_2C{-}C_{10}H_6{-}CO_2)_3$. *J. Am. Chem. Soc.* **2005**, *127*, 9376−9377.
(33) Senkovska, I.; Kaskel, S. Solvent-induced pore-size adjustment in the metal−organic framework $[Mg_3(ndc)_3(dmf)_4]$ (ndc = naphthalenedicarboxylate). *Eur. J. Inorg. Chem.* **2006**, 4564−4569.
(34) Rood, J. A.; Noll, B. C.; Henderson, K. W. Synthesis, structural characterization, gas sorption and guest-exchange studies of the lightweight, porous metal−organic framework α-$[Mg_3(O_2CH)_6]$. *Inorg. Chem.* **2006**, *45*, 5521−5528.
(35) Kaduk, J. A. Terephthalate salts of dipositive cations. *Acta Crystallogr., Sect. B: Struct. Sci.* **2002**, *58*, 815−822.
(36) Rood, J. A.; Noll, B. C.; Henderson, K. W. Cubic networks and 3^6 tilings assembled from isostructural trimeric magnesium aryldicarboxylates. *Main Group Chem.* **2006**, *5*, 21−30.
(37) Givaja, G.; Amo-Ochoa, P.; Gómez-García, C. J.; Zamora, F. Intrinsic electrical conductivity of nanostructured metal−organic polymer chains. *Chem. Soc. Rev.* **2012**, *41*, 115−147.
(38) Gándara, F.; Uribe-Romo, F. J.; Britt, D. K.; Furukawa, H.; Lei, L.; Cheng, R.; Duan, X.; O'Keeffe, M.; Yaghi, O. M. Porous, Conductive Metal-Triazolates and Their Structural Elucidation by the Charge-Flipping Method. *Chem. − Eur. J.* **2012**, *18*, 10595−10601.
(39) Lin, J.; Peng, Z.; Xiang, C.; Ruan, G.; Yan, Z.; Natelson, D.; Tour, J. M. Graphene nanoribbon and nanostructured SnO_2 composite anodes for lithium ion batteries. *ACS Nano* **2013**, *7*, 6001−6006.
(40) Maiti, S.; Dhawa, T.; Mallik, A. K.; Mahanty, S. CeO_2@C derived from benzene carboxylate bridged metal−organic frameworks: ligand induced morphology evolution and influence on the electrochemical properties as a lithium-ion battery anode. *Sustainable Energy Fuels* **2017**, 288.
(41) Chen, L.; Liu, Y.; Zhang, F.; Liu, C.; Shaw, L. L. PVP-assisted synthesis of uniform carbon coated Li_2S/CB for high-performance lithium−sulfur batteries. *ACS Appl. Mater. Interfaces* **2015**, *7*, 25748−25756.
(42) Wang, J.; Ma, R.; Zhou, Z.; Liu, G.; Liu, Q. Magnesiothermic synthesis of sulfur-doped graphene as an efficient metal-free electrocatalyst for oxygen reduction. *Sci. Rep.* **2015**, *5*, No. 9304.
(43) Qiao, S.-J.; Xu, X.-N.; Qiu, Y.; Xiao, H.-C.; Zhu, Y.-F. Simultaneous reduction and functionalization of graphene oxide by 4-hydrazinobenzenesulfonic acid for polymer nanocomposites. *Nanomaterials* **2016**, *6*, 29.
(44) Li, B.; Cao, H.; Yin, G. $Mg(OH)_2$@reduced graphene oxide composite for removal of dyes from water. *J. Mater. Chem.* **2011**, *21*, 13765−13768.
(45) McKelvy, M. J.; Sharma, R.; Chizmeshya, A. V. G.; Carpenter, R. W.; Streib, K. Magnesium hydroxide dehydroxylation: in situ nanoscale observations of lamellar nucleation and growth. *Chem. Mater.* **2001**, *13*, 921−926.
(46) Zeng, R.-C.; Li, X.-T.; Li, S.-Q.; Zhang, F.; Han, E.-H. In vitro degradation of pure Mg in response to glucose. *Sci. Rep.* **2015**, *5*, No. 13026.
(47) Fotea, C.; Callaway, J.; Alexander, M. R. Characterisation of the surface chemistry of magnesium exposed to the ambient atmosphere. *Surf. Interface Anal.* **2006**, *38*, 1363−1371.
(48) Rheinheimer, V.; Unluer, C.; Liu, J.; Ruan, S.; Pan, J.; Monteiro, P. XPS study on the stability and transformation of hydrate and carbonate phases within MgO systems. *Materials* **2017**, *10*, 75.
(49) Forsgren, J.; Frykstrand, S.; Grandfield, K.; Mihranyan, A.; Strømme, M. A template-free, ultra-adsorbing, high surface area carbonate nanostructure. *PLoS One* **2013**, *8*, No. e68486.
(50) Klose, M.; Pinkert, K.; Zier, M.; Uhlemann, M.; Wolke, F.; Jaumann, T.; Jehnichen, P.; Wadewitz, D.; Oswald, S.; Eckert, J.; Giebeler, L. Hollow carbon nano-onions with hierarchical porosity derived from commercial metal organic framework. *Carbon* **2014**, *79*, 302−309.
(51) Zhang, Z.; An, Y.; Feng, J.; Ci, L.; Duan, B.; Huang, W.; Dong, C.; Xiong, S. Carbon coated copper sulfides nanosheets synthesized via directly sulfurizing metal−organic frameworks for lithium batteries. *Mater. Lett.* **2016**, *181*, 340−344.
(52) Wang, Z.; Wang, B.; Yang, Y.; Cui, Y.; Wang, Z.; Chen, B.; Qian, G. Mixed metal−organic framework with effective Lewis acidic sites for sulfur confinement in high-performance lithium−sulfur batteries. *ACS Appl. Mater. Interfaces* **2015**, *7*, 20999−21004.
(53) Guo, J.; Xu, Y.; Wang, C. Sulfur-impregnated disordered carbon nanotubes cathode for lithium−sulfur batteries. *Nano Lett.* **2011**, *11*, 4288−4294.
(54) Fan, C.-Y.; Xiao, P.; Li, H.-H.; Wang, H.-F.; Zhang, L.-L.; Sun, H.-Z.; Wu, X.-L.; Xie, H.-M.; Zhang, J.-P. Nanoscale polysulfides reactors achieved by chemical Au−S interaction: improving the performance of Li−S batteries on the electrode level. *ACS Appl. Mater. Interfaces* **2015**, *7*, 27959−27967.
(55) Jiang, J.; Zhu, J.; Ai, W.; Wang, X.; Wang, Y.; Zou, C.; Huang, W.; Yu, T. Encapsulation of sulfur with thin-layered nickel-based hydroxides for long-cyclic lithium−sulfur cells. *Nat. Commun.* **2015**, *6*, No. 8622.
(56) Chen, S.; Huang, X.; Liu, H.; Sun, B.; Yeoh, W.; Li, K.; Zhang, J.; Wang, G. Encapsulating sulfur into highly graphitized hollow carbon spheres as high performance cathode for lithium−sulfur batteries. *Adv. Energy Mater.* **2014**, *4*, No. 1301761.

DOI: 10.1021/acsomega.7b01156
ACS Omega 2017, 2, 6481−6491

(57) Wang, C.; Su, K.; Wan, W.; Guo, H.; Zhou, H.; Chen, J.; Zhang, X.; Huang, Y. High sulfur loading composite wrapped by 3D nitrogen-doped graphene as a cathode material for lithium−sulfur batteries. *J. Mater. Chem. A* **2014**, *2*, 5018−5023.
(58) Zhang, S. S. Role of $LiNO_3$ in rechargeable lithium/sulfur battery. *Electrochim. Acta* **2012**, *70*, 344−348.
(59) Xu, G.; Ding, B.; Shen, L.; Nie, P.; Han, J.; Zhang, X. Sulfur embedded in metal organic framework-derived hierarchically porous carbon nanoplates for high performance lithium−sulfur battery. *J. Mater. Chem. A* **2013**, *1*, 4490−4496.
(60) Barbier, A.; Stierle, A.; Finocchi, F.; Jupille, J. Stability and stoichiometry of (polar) oxide surfaces for varying oxygen chemical potential. *J. Phys.: Condens. Matter* **2008**, *20*, No. 184014.
(61) Altieri, S.; Contri, S. F.; Valeri, S. Hydrolysis at MgO(100)/Ag(100) oxide-metal interfaces studied by O1s x-ray photoelectron and Mg $KL_{23}L_{23}$ Auger spectroscopy. *Phys. Rev. B* **2007**, *76*, No. 205413.
(62) Ma, Z.; Dou, S.; Shen, A.; Tao, L.; Dai, L.; Wang, S. Sulfur-Doped Graphene Derived from Cycled Lithium−Sulfur Batteries as a Metal-Free Electrocatalyst for the Oxygen Reduction Reaction. *Angew. Chem., Int. Ed.* **2015**, *54*, 1888−1892.
(63) Liang, X.; Hart, C.; Pang, Q.; Garsuch, A.; Weiss, T.; Nazar, L. F. A highly efficient polysulfide mediator for lithium−sulfur batteries. *Nat. Commun.* **2015**, *6*, No. 5682.
(64) Choi, C. H.; Park, S. H.; Woo, S. I. Heteroatom doped carbons prepared by the pyrolysis of bio-derived amino acids as highly active catalysts for oxygen electro-reduction reactions. *Green Chem.* **2011**, *13*, 406−412.
(65) Ponraj, R.; Kannan, A. G.; Ahn, J. H.; Kim, D.-W. Improvement of Cycling Performance of Lithium−Sulfur Batteries by Using Magnesium Oxide as a Functional Additive for Trapping Lithium Polysulfide. *ACS Appl. Mater. Interfaces* **2016**, *8*, 4000−4006.
(66) Manthiram, A.; Fu, Y.; Su, Y.-S. Challenges and prospects of lithium−sulfur batteries. *Acc. Chem. Res.* **2013**, *46*, 1125−1134.
(67) Zhang, S.; Zheng, M.; Lin, Z.; Li, N.; Liu, Y.; Zhao, B.; Pang, H.; Cao, J.; He, P.; Shi, Y. Activated carbon with ultrahigh specific surface area synthesized from natural plant material for lithium−sulfur batteries. *J. Mater. Chem. A* **2014**, *2*, 15889−15896.

DOI: 10.1021/acsomega.7b01156
ACS Omega 2017, 2, 6481−6491